

AN OPTIMAL TECHNIQUE FOR REALISING SRM ON ELECTRIC VEHICLES WITH HIGH SPEED VECTOR CONTROL

¹V GOPALA KRISHNA, ²A BHARGAV, ³V.ABHINAY, ⁴S M SHAFEE

^{1,2,3,4}Dept of Mechanical Engineering, Sree Venkateswara College Of Engineering, Nellore (Dt), Andhra Pradesh, India.

ABSTRACT

In an electric vehicle (EV), the high speed motor effectively lowers the motor. Switched Reluctance Motors (SRM) are suitable for high speed drives due to the simple and dependable rotor design. However, there is a disadvantage in that there is significant trembling and acoustic noise. The difficulty of constructing a torque controller is also exacerbated by the intricacy of the unipolar current excitation. The vector control has been suggested as a solution to these SRM issues. However, the SRM has not been subjected to vector control in the high speed zone. This research specifies the driving parameters, such as switching frequency and bus voltage, for applying vector control to the SRM in the high speed zone. The experiment shows that the recommended SRM is capable of realising high output power with less vibration in the high speed region and is controllable by vectors.

Keywords: Switched reluctance motor, high speed drive, Vector control

1. INTRODUCTION

Due to a growing uproar from environmental activists and government laws, petrol emissions must now be severely reduced due to their influence on the ozone layer [1]. Conventional transportation systems (vehicles) are powered by internal combustion engines (ICE), which affect the environment by releasing hydrocarbon oxides when petrol and fuel are burned. Research on renewable energy sources has advanced and evolved alongside the development of hybrid electric vehicles (HEVs), which move their wheels using both internal combustion engines and electric motors [2-4]. Fully electric cars (EVs) have also been available and in use since that period [5]. These vehicles are propelled by one or more electric motors [6]. Researchers are presently looking into the use of renewable energy sources including sun, wind, and tidal waves for sustainable transportation [7-10].

The energy supply, auxiliary, and electronic propulsion subsystems are the main three components that make up an electric vehicle [3,11,12]. The power converter, the mechanical gearbox, the electric motor, and the electronic controller make up the electronic propulsion subsystem. The numerous electric automobile motors that are on the market are summarised in this article (Fig. 1).

Electrical drives took shape with Faraday's demonstration of electromagnetic induction in the 18th century [14]. Faraday's law led to the development of electric motors, which include the alternating current and direct current motor types.

Rotor, stator, windings, air gap, and commutators or converters are common components of an electric motor. Numerous types of electric motors are built on the basis of different arrangements of these parts [15]. Brushless permanent magnet motors are electric motors that do not require brushes for commutation or energy conversion [16]. The rear Electromotive Force (rear-EMF) of a motor may also be used to categorise it. They could have a sinusoidal or a trapezoidal shape. Depending on how they are constructed and how energy is transferred, they may either be Permanent Magnet AC Synchronous Motors (PMSM) or Brushless DC Motors (BLDC) [17].

An electric motor must be highly efficient, have a high power density, and be reasonably priced to be successfully used as the drive for EVs [11]. In addition, unlike industrial motors and conveyors, EV motor drives demand frequent starts and stops, rapid acceleration and deceleration, high torque at low speeds, low torque at high speeds, and a broad speed range. The motor's specification, though, is based on its intended use. This application encompasses systems for light-duty, conventional, and residential automobiles. Additionally, the duty cycle, thermal properties, and cooling system used by the vehicle all affect motor performance [11]. The Figure categorizes the numerous traction motors that are employed. Below is a brief review of the literature on the EV/HEV traction motors. Based on the properties indicated previously, a literature evaluation of both AC and DC motors is offered in this paper.

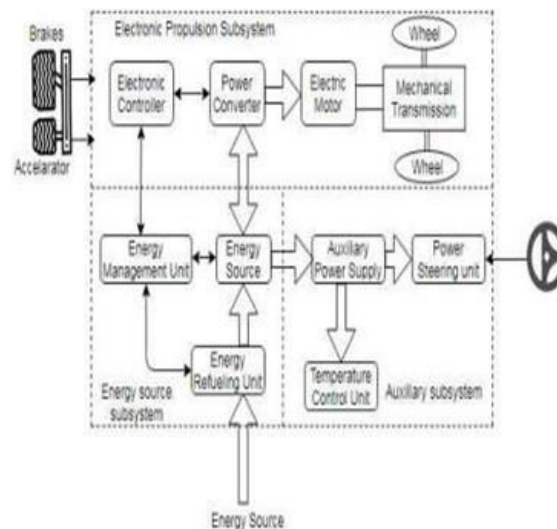


Fig. 1. Block diagram of an electric vehicle [13]

2. RELATED WORK

Despite not utilising costly permanent magnets, switched reluctance motors are faster than stepper motors. It combines the positive aspects of an AC induction motor, a brushless motor, and a DC motor. For applications requiring more torque and faster speeds, the SRM is also a cost-effective substitute for existing synchronous and induction machines (Li et al. 2019). Air pollution has been a major environmental problem over the last few decades. The majority of air pollution is caused by the gasoline that cars use. In terms of the environment, electric cars are dependable for lowering air pollution levels (Suresh et al. 2020; Karthik et al. 2020; Subasri et al. 2020; Sheela et al. 2020). The switching reluctance motor (SRM) is used in the majority of electric car manufacturing. Due to their specialised qualities, SRMs are utilised in electric cars (Aiso, Takahashi, and Akatsu 2019).

Conventional SRMs exhibit all of these traits, but they also have some disadvantages, such as noise, magnetic saturation, and torque ripples (Qianfan, Shumei, and Xinjia 2007). Their activities' subpar efficiency is caused by all of these factors. Despite having some drawbacks, researchers develop a variety of topologies with special and distinguishing characteristics in order to increase their efficacy.

An alternate approach to raising the torque profile has been put out in, where effective optimisation of the design has been done and the reasons that prevent its widespread use have been highlighted. A novel topology called the double rotor was proposed by Qianfan, Shumei, and Xinjia (2007) to increase efficiency. A synchronous machine and a traditional SRM are both hallmarks of the unique dual-mode SRM (Miller 1989). According to Sun et al. (2019), increasing the number of rotor poles is another efficient technique to increase torque, but doing so results in a larger design and a more expensive machine.

The rotor poles of the SRM were modified by Li, Ravi, and Aliprantis (2016) to reduce magnetic saturation and increase torque. In this study, a unique topology is created, and the typical SRM's stator poles are modified to enhance the torque profile and reduce material bulk. In the recommended topology, a portion of the core material is removed to form a slotted stator tooth at a certain depth. The winding of the suggested SRM motor is similar to that of the conventional design.

Vector Control for SRM's Controllability

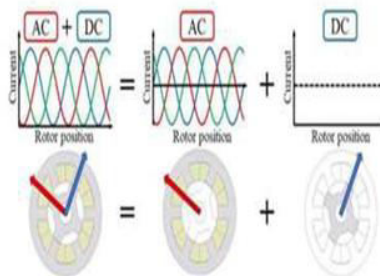


Fig.2. SRM Vector Control

Figure illustrates the SRM's vector control. This stimulates the subject using a three-phase sinusoidal DC offset current. The rotating magnetic field is created by the stator's current component. The direct current component, which generates a magnetic flux vector, is positioned depending on where the rotor is placed. The rotor field vector is a representation of the magnetic stream that flows through it. By interacting with the magnetic flux of the rotor and the revolving magnetic field of the stator, torque can be produced.

Mathematical calculations are used by the SRM's vector control system to produce torque.

In the equivalent SRM's voltage equation, the zero-phase volume is represented by the d-q axis. This equation defines the self-inductance of a wire coil in terms of zero-phase voltage and a DC component of the voltage along the d-axis, a zero-phase volume, and a zero-phase voltage component.

By deducting the DC component from the total current, it is possible to get the zero-phase component of the excitation current (3). By using the second term of the inductance matrix (2), which is denoted by the following formula: The letter I in the symbol stands for the virtual rotor's inertia. Figure demonstrates how virtual rotor flows are produced as a function of time by zero-phase current. The equation used to calculate the SRM torque is as follows: In other words, there are two opposing viewpoints on this matter. (5) There are more than twice as many persons as there were before who have no queries. If I had to guess, I would say that when we compare zero-phase currents to rotational torque and flux currents, we find that they are extremely close in terms of magnitude and frequency.

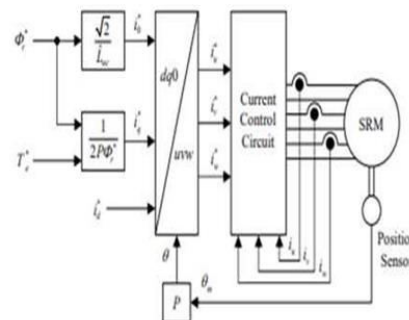


Fig.3. Vector Control System for SRM Drive

The current controller is thoroughly investigated. Figure shows the vector control controllers that are currently on the market. shows the PI controller that is now in use, the disconnecting controller, and the feed forward

controller. A carrier-based PWM inverter can handle those controllers' voltage commands. Every axis and phase of the circuit's current flow must be kept under control by the PI controller. It has a time constant of one tenth of a second, which is extremely fast. The managed SRM can be recognized as the rotating reference framework's RL circuits as a result of decoupling and forward control mechanisms. For the optimal single order current response, make sure that c equals the controlled machine's time constant (Ldc/R), as shown in the diagram. The Kc gain is established by the present response speed of a system under consideration. One of the goals of this research is to duplicate and test an existing controller.

3. PROPOSED SRM

The specifications for the two SRMs shown in Figure, one with a 12-pin layout and eight poles and the other with a 30-pin layout with twenty poles, are shown in Table I. The smaller of the two SRMs is the 12-pin with eight poles model. In order to demonstrate controllability at high rotating speeds, it was crucial to take into account that the 20-pole, 30-slot SRM would share the same electric angular frequency and electrical properties as the 8-pole, 12-slot SRM.

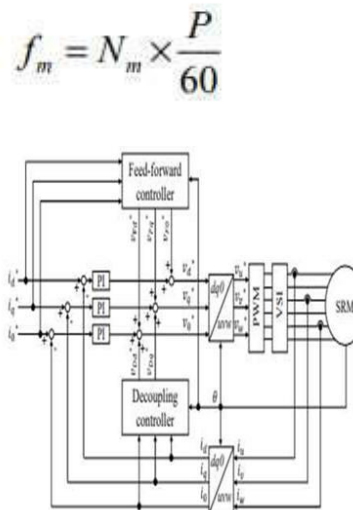


Fig.4. current vector control controller

B. High-speed drive controllability

These factors define the switching frequency, bus voltage, necessary power, and required 20000 rpm rotational speed. At 20,000 revolutions per minute and a reference torque of 16.2 Nm, the simulation analyses the current and torque waveforms. The waveforms of the current and torque in relation to the switching frequency are shown in Figure. The frequency at which the switch is made has an impact on the harmonic distortion and current wave ratio. Current ripple ratio (CRR) and effective value of the harmonic current order are terms that are used to describe harmonic distortions (I1). The variables i_{max} , i_{min} , and i_{ave} , which stand for maximum, minimum, and average, respectively, provide the current amplitudes at their maximum, minimum, and average values. Table II displays an A q-axis, zero-phase THD, and current rippling ratios for the switching frequency, which is likewise displayed in Figure. According to Figure and Table, switching frequency lowers as switching frequency increases, and THD and current ripple rate also drop as switching frequency increases. Total harmonic distortion (THD) must be kept to a minimum since high-speed motor harmonic fluxes cause an increase in iron loss..

4. SIMULATION RESULTS

An electric motor has a maximum rotational frequency of $60 P f N (1)$, where P is the number of poles, f_m is the maximum electric frequency, and N_m is the maximum rotational frequency. The greatest electrical frequency at which the Model A can function in compliance with the specifications is 6.67 kHz (1). There is also a twenty-pole model available that can rotate at a maximum rate of 20,000 revolutions per minute, the same as the Model A. The exterior diameter, stack length, air gap length, and inner diameter of both SRMs are identical. Additionally, their auto-inductance distributions show nearly the same variance as the distributions shown in Figure. In order to estimate the SRM torque, use the following calculation:

$$T = \frac{P}{2} \frac{\partial L}{\partial \theta} i^2$$

In the equation $P L T I (2)$, the words torque output, inductance, electric angle, and current are represented, respectively, by the letters P , L , and I . With more poles, the torque increases linearly (2). The Model B has a torque that is 2.5 times more than the Model A. The current consumption of Model B should need to be increased by 0.63 times in order to provide the same amount of torque as Model A. Figure illustrates the features of the situation as it stands right now. Torque is referred to by the acronym "torque." When no magnetic saturation area is installed with the same current as the Model A torque, Model B torque is 2.5 times stronger than Model A torque (see Fig).

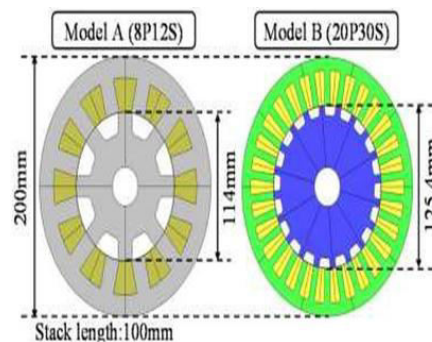


Fig.5. Motor structure of the proposed SRMs.

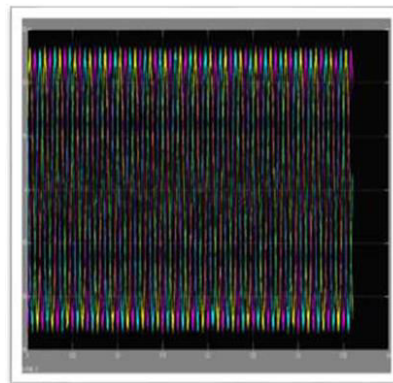


Fig.6. Current-Torque characteristic.

TABLE I
 SPECIFICATION OF PROPOSED SRM

	Model A	Model B
Pole / Slot	8 / 12	20 / 30
Output power [kW]	85	34
Maximum speed [rpm]	50000	20000
Air gap length [mm]	0.5	0.5
Number of turns [turn/teeth]	5	5
Diameter of coil [mm]	6.0	4.0
Resistance [Ω /phase]	0.003	0.018
Core material	-	20H1200

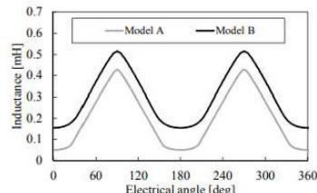


Fig. Self-inductance waveforms of the proposed SRMs.

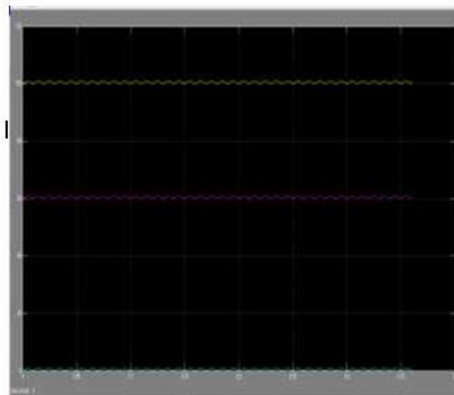
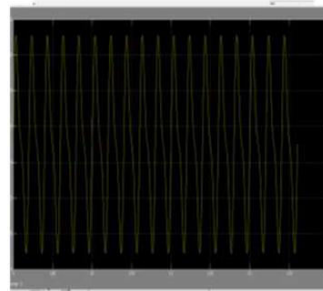
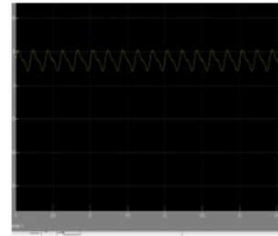
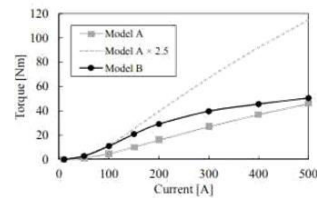


Fig.7. Waveforms of the planned SRMs' self-inductance.

CONCLUSION

This study built and evaluated a 20-pole 30-slot SRM that is driven at 20000 rpm and has the same electrical angular frequency as an 8-pole 12-slot SRM that is driven at 50000 rpm in order to apply vector control to the SRM in the high speed drive. To fulfil the torque and output power demands of the vector control system, the suggested motor used a SiC inverter with a 200kHz switching frequency.

The experiment demonstrated that the recommended SRM can be driven by vector control at 20,000 rpm, the maximum spinning speed. This shows that the 8-pole, 12-slot SRM can be driven by the vector control at a speed of 50,000 rpm. Finally, it was shown that using vector control instead of the more traditional single pulse drive can reduce SRM vibration in the high speed region.

REFERENCES

1. M. Besharati, J. Widmer, G. Atkinson, V. Pickert, Jamie Washington : “Super-high-speed switched reluctance motor for automotive traction”, IEEE Energy Conversion Congress and Exposition (ECCE), pp.5241-5248, September 2015.
2. Earl W. Fairall, Berker Bilgin, Ali Emadi :“State-of-the-Art High-speed Switched Reluctance Machines”, IEEE International Electric Machines and Drives Conference (IEMDC), pp.1621-1627, May 2015.
3. M. N. Anwar and Iqbal Husain, “Radial Force Calculation and Acoustic Noise Prediction in Switched Reluctance Machines” IEEE Transaction on Industry Application, Vol.36, No.6, pp.1589-1597, 2000.
4. Chenjie Lin and Babak Fahimi, “Prediction of Radial Vibration in Switched Reluctance Machines”, IEEE Transaction on Energy Conversion, pp.250-258, Vol.29, No.1, 2014
5. H. Makino, T. Kosaka, Nobuyuki Matsui, “Digital PWM Control-Based Active Vibration Cancellation for Switched Reluctance Motors”, IEEE Transaction on Industry Application, Vol.51, No.6, pp.4521-4530, Nov 2015.
6. A. Tanabe, K. Akatsu, “Vibration reduction method in SRM with a smoothing voltage commutation by PWM”, 9th International Conference on Power Electronics and ECCE Asia (ICPE-ECCE Asia), June 2015.
7. K. M. Rahman, B. Fahimi, G. Suresh, A. V. Rajarathnam, and M. Ehsani, "Advantages of Switched Reluctance Motor Applications to EV and HEV: Design and Control Issues," IEEE Transactions on Industry Applications, vol. 36, No. 1, pp. 111-121, January/February 2000.
8. I. Husain and S. A. Hossain, "Modeling, Simulation, and Control of Switched Reluctance Motor Drives," IEEE Transactions on Industrial Electronics, vol. 52, No. 6, pp. 1625-1634, December 2005.
9. N. Nakao, K. Akatsu, “Vector control specialized for switched reluctance motor drives”, International Conference on Electrical Machines (ICEM), pp.943-949, September 2014.
10. N. Nakao, K. Akatsu, “Vector control for switched reluctance motor drives using an improved current controller”, IEEE Energy Conversion Congress and Exposition (ECCE), pp.1379-1386, Sept 2014.